Molecular Therapy
Methods & Clinical Development
Original Article

Impact of cell culture transition on adipose-derived mesenchymal stromal cells: Multi-omics analysis of small- vs large-scale production

Marina Ramírez Galera,[1] Athanasios Oikonomou,[2] Jonas D. Elsborg,[3] Lisa Harth,[1] Anne Fischer-Nielsen,[6] Marianne Bengtson Løvendorf,[1,4,5] Beatrice Dyring-Andersen,[1,3,5] Francesco Iorio,[2] Lea Munthe Fog,[6] Anders Woetmann,[1] and Jesper Dyrendom Svalgaard[6]

[1]The LEO Foundation Skin Immunology Research Center, Department of Immunology and Microbiology, Faculty of Health and Medical Sciences, University of Copenhagen, Copenhagen, Denmark; [2]Computational Biology Research Centre, Human Technopole, Milan, Italy; [3]Proteomics Program, Novo Nordisk Foundation Center for Protein Research, Faculty of Health and Medical Sciences, University of Copenhagen, Copenhagen, Denmark; [4]Department of Dermatology and Allergy, Copenhagen University Hospital - Herlev and Gentofte, Hospital, Hellerup, Denmark; [5]Department of Dermatology, Zealand University Hospital, Roskilde, Denmark; [6]Celcore ApS, Soeborg, Denmark

Mesenchymal stromal cells (MSCs) are being tested in numerous clinical trials, yet the limited progression of these trials to advanced stages indicates unresolved translational challenges. Expanding MSCs is a critical step in most therapeutic applications, and bioreactor-based culture offers large-scale production compared to monolayer cultures. Nevertheless, since MSCs sense their microenvironment, it is crucial to understand how these systems affect their properties. We expanded human adipose-derived mesenchymal stromal cells (AD-MSCs) from the same donors in both small- and large-scale platforms. Bulk-RNA sequencing (RNA-seq) and mass spectrometry analysis demonstrated that small-scale culture had a broader range of differentially expressed genes (DEGs) and proteins within immunomodulatory, cell migration, and cell adhesion pathways. In contrast, the large-scale culture showed a lower amount of DEGs and proteins associated mainly with extracellular matrix synthesis. Our findings demonstrate that expansion platforms significantly impact MSCs' properties, highlighting the need to optimize expansion conditions to obtain high cell yield without compromising MSCs' attributes.

INTRODUCTION

Mesenchymal stromal cells (MSCs) have emerged as a promising tool in regenerative medicine and cell-based therapies due to their unique properties, including multilineage differentiation potential, immunomodulatory effects, and ability to secrete bioactive molecules.[1,2] While more than a thousand clinical trials using MSCs are currently registered worldwide (ClinicalTrials.gov), the limited progression to late stages trials underscores unresolved translational challenges.[3,4]

Progressing through clinical trials often involves the need to transition from small-scale laboratory cultures to large-scale systems, e.g., bioreactor-based production. This shift in culture platforms is crucial for generating sufficient cell quantities for therapeutic use, improving cost effectiveness and reducing media consumption. However, the transition from traditional two-dimensional adherent cultures to large-scale systems presents several challenges that must be carefully considered. Given that MSCs can sense and respond to their microenvironment, it is crucial to understand the impact that this expansion platform has on MSCs' properties.[5–8] Changes in the cellular microenvironment can alter gene expression- and proteomic profiles, as well as the secretion of factors that can potentially lead to changes in cell potency such as differentiation capacity, angiogenic profile, or immunomodulatory properties. While bioreactors have demonstrated to provide a higher cell yield retaining MSCs cell viability, cell surface marker expression, and differentiation potential,[8–11] few studies have reported the impact that large-scale expansion has on MSCs' properties and on their therapeutic effect.[12,13] Therefore, the effects of large-scale expansion on MSCs' attributes remain largely unexplored, and the current studies are insufficient to fully understand its impact.

This study aims to explore the effect that transitioning between culture systems may have on adipose-derived mesenchymal stromal cells' (AD-MSCs) properties, focusing on the potential changes in cell transcriptome and proteome profiles. Our findings suggest that switching culture platform, in our setting, has a significant impact on AD-MSCs' properties, highlighting the need to optimize expansion conditions not only to increase cell yield but also to preserve the attributes of MSCs.

Received 13 January 2025; accepted 10 June 2025;
https://doi.org/10.1016/j.omtm.2025.101512.

Correspondence: Marina Ramírez Galera. The LEO Foundation Skin Immunology Research Center, Department of Immunology and Microbiology, Faculty of Health and Medical Sciences, University of Copenhagen, Copenhagen, Denmark.
E-mail: marina.galera@sund.ku.dk

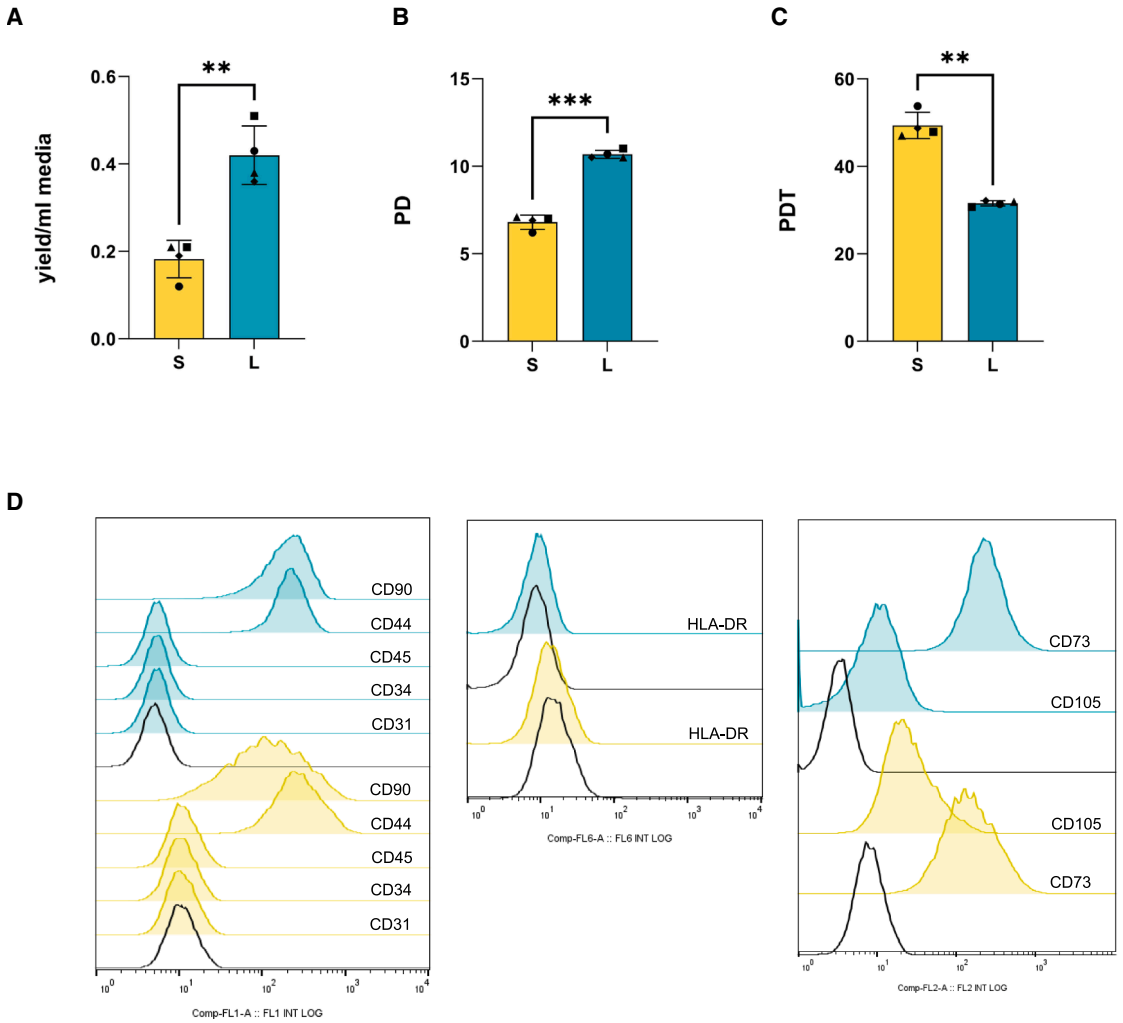

(legend on next page)

RESULTS

Large-scale platform produces higher AD-MSCs yield without significantly affecting differentiation potential and surface markers expression

We established two parallel cell culture platforms for expansion of human AD-MSCs: a small-scale flask-based platform (S) and a large-scale bioreactor platform (L). To ensure comparability, identical media formulation, oxygen tension and temperature were maintained across both platforms.

The L platform produced a 2-fold higher AD-MSCs yield/mL media compared to the S platform (Figure 1A). This resulted in a correspondingly higher number of population doublings compared to those in the S platform (median values of 10.6 and 6.95, respectively), resulting in an overall more rapid proliferation in the L platform observed as a decrease in PD time (median values of 31.7 and 48.3 h, respectively) (Figures 1B and 1C). We next compared the canonical MSCs surface markers and differentiation potential on cells from each platform. The cells derived from both platforms showed positive expression of CD44, CD73, CD90, and CD105, while showing lack of expression of CD45, CD34, CD31, and HLA-DR molecules (Figures 1D and 1E). Additionally, cells from both cultures retained differentiation capacity and demonstrated the ability to differentiate into adipocytes, osteoclasts, and chondrocytes (Figure S1). These results confirm that both platforms produced cells meeting the essential characteristics defining AD-MSCs, according to The International Society for Cellular Therapy (ISCT) criteria.[14,15]

Culture platform influences AD-MSCs transcriptional and proteomic profile

To gain deeper insights into potential molecular differences beyond proliferation and multipotency, we conducted bulk-RNA sequencing (RNA-seq) on AD-MSCs cultured in both platforms. Our analysis identified 927 differentially expressed genes (DEGs) between the two culture methods, based on thresholds of |log2 fold change| >2 and a Benjamini-Hochberg adjusted p-value <0.05. (Figure 2A; Table S1). The heatmap revealed 565 downregulated genes and 362 upregulated genes in the L platform compared with the S platform (Figure 2A). These results underlined that AD-MSCs cultured in S platform have a broader gene transcription profile. We observed, as expected, donor-to donor variability in both culture platforms.

Principal-component analysis (PCA) on the expression of the 927 DEGs confirmed the two transcriptionally distinct subgroups based on culture method (Figure 2B), with the first principal component explaining ∼64% of the total variability in the data. This distinct separation demonstrates that the culture method influences AD-MSCs' transcriptional profile. Interestingly, AD-MSCs cultured in the L platform clustered more closely together than those grown in the S platform, suggesting that the large-scale cultures are transcriptionally more homogenous.

Subsequently, we performed an active-subnetwork-oriented pathway enrichment analysis to identify pathways and gene terms of DEGs, which based on STRING database are shown to interact, thus implying altered gene expression in distinct biological networks. In this way, we unraveled 631 interacting genes within the pool of 927 DEGs with an upregulation in either culture method (Table S2), and proceeded with enrichment analysis focusing on gene ontology (GO) gene sets of "biological process (BP)" and "molecular function (MF)" with a Benjamini-Hochberg adjusted p-value <0.05 (Table S3). Interestingly, GO-BP and GO-MF enrichment analysis highlighted gene terms associated with immunomodulation, extracellular matrix (ECM) synthesis, cell adhesion and remodeling, as well as cell migration (Figures 2C and 2D). Among these, GO-BP_cell_chemotaxis and GO_MF_integrin_binding were the most significant pathways, whereas GO-BP_antigen_processing_and_presentation_of_exogenous_peptide_anigen_via_mhc_class_II and GOMF_extracellular_matrix_structural_constituent had the highest fold enrichment (∼3-fold and ∼5-fold, respectively).

To further characterize the genes upregulated within AD-MSCs cultured in either S or L platforms, we generated a heatmap of the DEGs from gene set enrichment analysis (GSEA) selected pathways (Figure 2E). AD-MSCs cultured in S platform had a more diverse gene profile associated with immunomodulatory pathways such as GOBP_CELL_CHEMOTAXIS (Figure 2E). Correspondingly, upregulation of chemokines such as *CCL3* and *CCL18*, chemoattractant for both innate and adaptive immune cells such as macrophages, and T lymphocytes was detected. Moreover, the higher expression of several chemokine receptors *CCR1*, *CCR5*, *CXCR4*, and *XCR1* on AD-MSCs cultured in the S platform suggests higher potential migratory capacity of AD-MSCs toward inflamed tissue, and the upregulation of alarmin interleukin *(IL)-33* and other cytokines (*IL-34* and *SPP1*). Besides, genes associated with antigen processing and presentation pathways are only upregulated in the S culture platform. In contrast, the AD-MSCs cultured in large-scale bioreactor upregulated genes involved in recruiting neutrophils (*CXCL1*, *CXCL2*, *CXCL3*, *CXCL5*, and *CXCL6*) and acute inflammation (*IL-1A* and *IL-1B*) (Figure 2E). These results suggest that in

Figure 1. Quantitative assessment of cell expansion in each culture platform

(A) Cell yield per mL of media of small-scale cultured AD-MSCs (S) and large-scale cultured AD-MSCs (L). (B) Population doubling (PD) of S and L cultured AD-MSCs. (C) PD time (PDT) of S and L cultured AD-MSCs. $^{**}p < 0.001$ and $^{***}p < 0.0005$ (D) Flow cytometry histograms illustrating the expression of phenotypic markers in AD-MSCs for each culture platform. Yellow: small-scale platform; blue: large-scale platform. Histograms show fluorescence intensity confirming the characteristic surface marker profile of AD-MSCs according to ISCT criteria. (E) Quantification of flow cytometry data showing the frequency of marker-positive cells. Bars represent the mean percentage of positive cells from three independent samples ($n = 3$), with error bars indicating standard deviation. Data were analyzed using FlowJo software. Negative gates were established using unstained samples or fluorescence minus one (FMO) control. Positive gates were set to contain no negative signal.

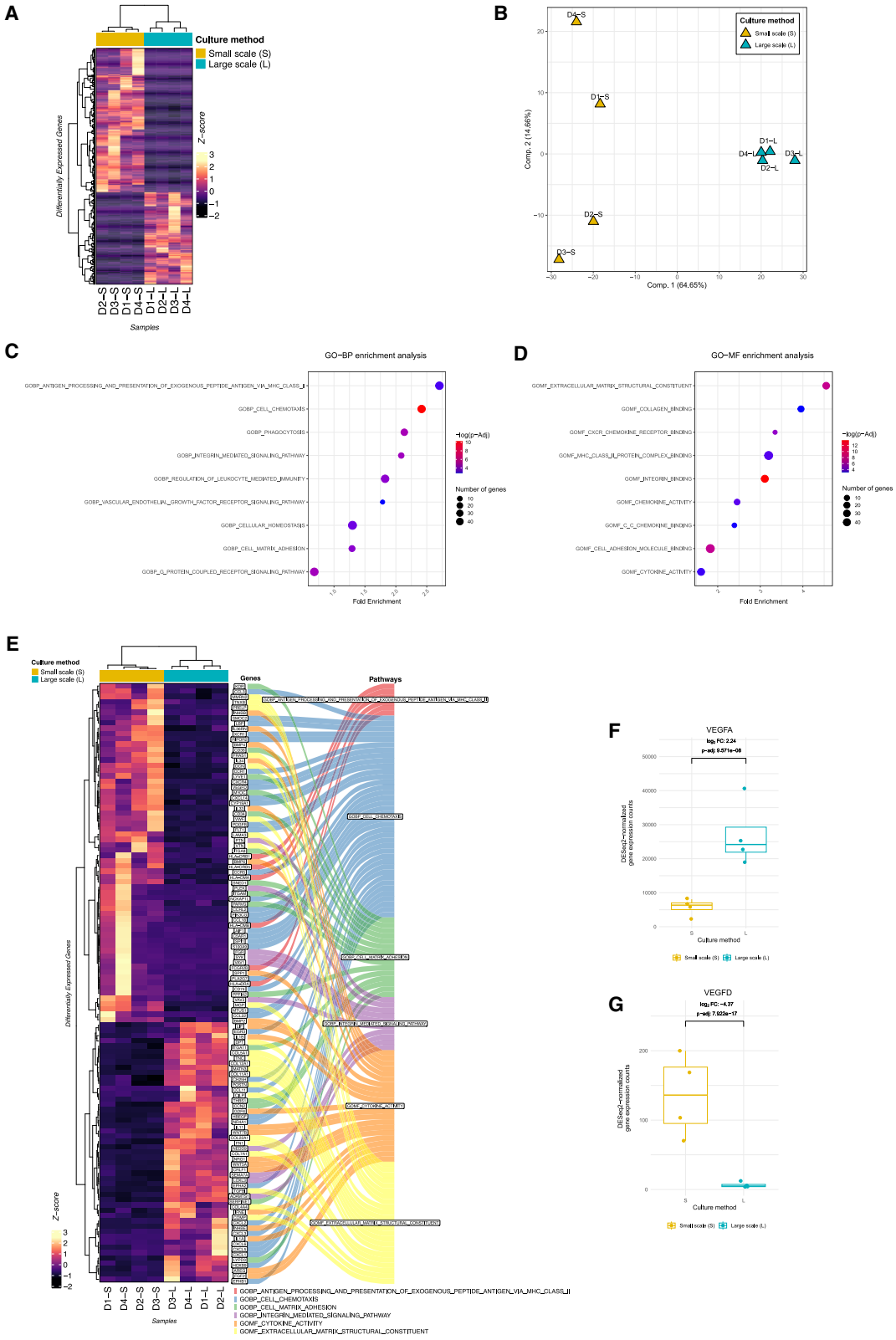

(legend on next page)

transition from S to L platform, the immunomodulatory profile of AD-MSCs becomes more restricted.

Differential regulation was also observed in pathways associated with the ECM (Figure 2E). In the L platform, multiple genes were upregulated including collagen coding genes (*COL11A1*, *COL12A1*, *COL22A1*, *COL4A4*, *COL5A1*, and *COL7A1*); essential ECM components (*TCN*, *POSTN*, *DPT*, and *MATN3*); adhesion molecules (*CCN2* and *THBS1*); and genes involved in ECM interaction and remodeling through integrin signaling (*ITGA11*, *LOXL3*, and *ADAMTS1*). Whereas genes involved in ECM remodeling and regulation (*MMP2*, *FRAS1, DCN*, *VTN*, and *PRELP*), adhesion (*CD34*, *CD36*, and *LYVE1*), and cellular motility as well as immune modulation (*ITGA8*, *ITGAM*, *FLT4*, and *FGR*) were downregulated.

Interestingly, in both culture platforms, differential upregulation of growth factors-related genes involved in wound healing and tissue repair (*PDGFB*, *VEGFD*, and *KDR* for S platform and *FGF2*, *AREG*, and *HBEGF* for L platform) was observed (Figure 2E). AD-MSCs produce the main pro-angiogenic factor *VEGFA*.[16,17] Interestingly, *VEGFA* expression is increased in large scale, whereas *VEGFD* expression is decreased when compared with small scale expression (Figures 2F and 2G). While *VEGFA* is associated with promoting angiogenesis, *VEGFD* is primarily linked to lymphangiogenesis.[16]

To validate bulk-RNA-seq results at the protein level, we performed bulk-mass spectrometry-based proteomic analysis on AD-MSCs from S and L cultures (details provided in materials and methods section). We quantified 1,034 differentially expressed proteins (DEPs) between the two culture platforms. In agreement with the transcriptomics analysis, PCA plot on the differential proteome expression showed a clear separation of each expansion platform group on the first two principal components (accounting for ∼68% of data variability), confirming that the expansion method impacts the proteome profile of AD-MSCs (Figure 3A). Consistent with bulk RNA-seq data, the L platform showed less variability in protein expression compared to S platform, as shown by a smaller coefficient of variance for this group (Figure S2). Likewise, unsupervised hierarchical heatmap on the 1,034 DEPs showed that L platform upregulated just 276 proteins compared to 758 proteins from the S platform (Figures 3B; Table S4). This indicates that AD-MSCs cultured in L platform have a more restrictive proteomic profile compared to AD-MSCs expanded on the S platform.

To gain a deeper understanding of the proteomic profiling of each group, we selected DEPs based on the GSEA transcriptomic results (Figure 3C). The heatmap showed that most of the selected proteins are downregulated in L platform. AD-MSCs expanded in L platform expressed proteins related to ECM synthesis and structural integrity (COL12A1, COL5A1, COL7A1, and COL11A1), as well as ECM degradation (MMP9), which indicates a dynamic balance between ECM production and degradation. In contrast, S cultured AD-MSCs expressed significantly more metalloproteinases (ADAM10, ADAMTS5, MMP2, and MMP14), highlighting a cellular shift in involvement in ECM degradation and remodeling in this setting (Figure 3C).

In line with transcriptomic results, AD-MSCs cultured S platform expressed HLA-I and HLA-II molecules -(Figure 3C) and showed elevated expression of proteins involved in inflammatory responses (IL-33 and CATG); immune regulation (LGALS3 and LGALS9) and cell migration (CCR1 and ACKR3); and antiviral and antimicrobial responses (STING, DEFA3, TLR3, and CAMP). Additionally, these cells expressed TGFB2, a multifunctional cytokine that influences many biological processes within tissue homeostasis, immune modulation, fibrosis, and wound healing. Moreover, expressions of cell adhesion and migration molecules (PDPN and ITB3) and growth factor receptors (TGFR2, PDGFRA, and PDGFRB) were also observed (Figure 3C). Taken together, these results indicate that platform transition induces a distinct phenotypic shift in AD-MSCs, characterized by two major changes: a reduction in immunomodulatory pathway complexity and enhanced expression of ECM-related genes and proteins. This alteration from a broad immunomodulatory profile to a more focused ECM-regulatory signature demonstrates the substantial influence of culture conditions on AD-MSCs molecular characteristics.

Integration of DEGs and proteins revealed a strong correlation (Spearman correlation coefficient = 0.74, p-value = $2.2e^{16}$) between gene expression and protein abundance (Figure 3D), confirming the consistency between transcriptional and translational regulation in our comparative analysis.

Given that our proteomes were analyzed from cell pellets, and thus did not capture any factors which may have been secreted from the cells, we performed a multiplex assay using Meso Scale Discovery (MSD) technology to analyze the levels of secreted factors in the media expressed by AD-MSCs cultured in both platforms (Figure 4). We

Figure 2. Distinct transcriptional signatures of AD-MSCs across the two culture methods

(A) Heatmap with hierarchical clustering illustrating the expression of the 927 differentially expressed genes (DEGs) (in rows; color gradient relevant to row-wise Z score of gene expression) across all donor samples belonging to each culture method (in columns). (B) Principal-component analysis using the DESeq2-normalized expression of the 927 DEGs between small (S; yellow triangles) versus large (L; blue triangles) culture method donor samples. (C and D) Gene ontology (GO) terms of (C) biological process (BP) and (D) molecular function (MF) identified upon the active-subnetwork-oriented pathway enrichment analysis of all the DEGs identified. Fold enrichment for each term (x axis) is supported by adjusted p-value statistical significance (color gradient), while the number of genes within each term is highlighted with dot size. (E) Heatmap with hierarchical clustering illustrating the expression of selected DEGs (in rows; color gradient relevant to row-wise Z score of gene expression) across all donor samples belonging to each culture method (in columns), with the alluvial plot on the right-hand side representing the enrichment in GO terms for these genes. (F and G) Boxplots illustrating the difference in DESeq2-normalized gene expression of *VEGFA* (F) and *VEGFD* (G) between samples (in dots) of the different culture scales (S: yellow: L: blue). Values for log2 fold change and adjusted p-value after the differential expression analysis on DESeq2 are indicated.

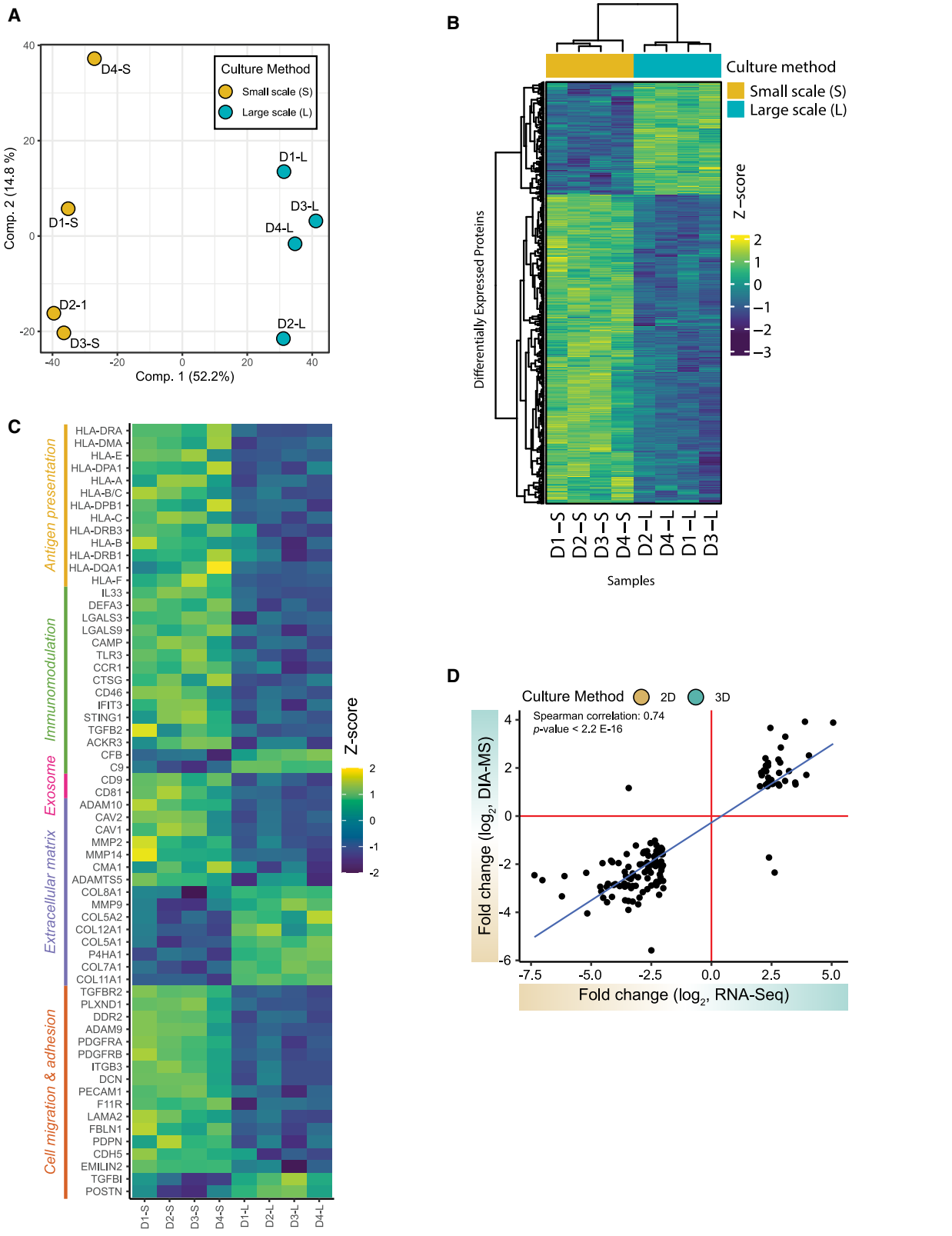

(legend on next page)

focused on a panel of cytokines and chemokines known to play significant roles in tissue repair and immune responses, specifically eotaxin, GM-CSF, IL-10, IL-13, IL-6, MCP-1, MIP-1α, MIP-1β, TSLP, tumor necrosis factor α (TNF-α), IL-8 (IL-8p and IL-8c), and VEGF.[18,19] Our analysis revealed that all measured soluble factors, except for eotaxin, TSLP and MCP-1, were significantly increased in AD-MSCs expanded in the S platform, reinforcing that AD-MSCs cultured in small-scale have a broader immunomodulatory profile. Contrary to RNA-seq results, VEGF-A exhibited similar expression levels in both culture platforms, suggesting that culture platform affects *VEGFA* transcriptional regulation, as we observed more abundant transcripts for L cultured AD-MSCs (Figure 2F); however, this does not translate in higher level of protein.

DISCUSSION

Transitioning from early to late-stage clinical trials often involve a switching of culture systems to meet the demand for increased cell numbers and more cost-effective production. Despite efforts to maintain identical culture media and parameters, this may not be sufficient to ensure the same cell product in terms of potency. Identifying these effects is critical, as they may contribute to challenges encountered in clinical translation.[8–11] This study explored transitioning between culture systems, focusing on the potential changes in cell transcriptome and proteome profiles.

Our findings highlight that the transition from small-scale (S) to large-scale (L) culture platforms can significantly influence the transcriptomic, proteomic and secretory profiles of AD-MSCs, even when using similar culture parameters. Notably, impacting distinct gene and protein expression patterns that are relevant to the therapeutic functions of MSCs. Especially the immunomodulatory properties, a key trait of AD-MSCs, was affected when changing the culture platform.

Contrary to flow cytometry results (Figures 1D and 1E) where cells showed lack of expression of HLA-DR in both culture platforms, transcriptomic and proteomic results showed that S-scale cultured cells expressed higher levels of both HLA-I and -II molecules, including HLA-DR, potentially making L-scale cultured AD-MSCs less immunogenic when injected into recipients. Compared to flow cytometry, mass spectrometry offers higher sensitivity, which could explain the detection of the HLA-DR molecule. The increased expression of HLA-I and -II molecules could hinder allogeneic MSCs administration as it can lead to transient immune reactions in immunocompetent recipients.[20] On the other hand, the activation of cytotoxic $CD8^+$ T cells, natural killer cells, and macrophages leads to MSCs apoptosis, which could trigger efferocytosis and promote immunosuppression.[21] Moreover, the expression of HLA molecules in itself does not necessarily induce immune activation, as this is highly dependent on co-expression of co-stimulatory molecules such as CD80 and CD86.[22,23] Importantly, we did not find expression of these molecules in our analysis.

The primary immunomodulatory and regenerative molecules produced by MSCs are paracrine factors such as chemokines, cytokines, growth factors, and extracellular vesicles (EVs). The secretome from MSCs can attract immune cells to sites of injury, contribute to tissue regeneration, and supress inflammation.[24] In our study, we observed a higher secretion of chemokines that attract immune cells from both the innate and adaptive immune system in S culture, while L-cultured AD-MSCs have a higher expression of chemokines involved only in neutrophil chemoattraction. One factor influencing MSCs therapeutic efficacy is AD-MSCs migration and recruitment into tissue.[25] *CXCR4* expression is detected in S-cultured AD-MSCs. Of note, it was demonstrated that MSCs positive for CXCR4 are able to home to injured tissue such as ischemic myocardium, brain lesions, and burn wounds, where its ligand CXCL12 is being secreted.[25] We were able to detect other chemokine receptors, especially in the S-platform. However, considering transcriptomic results, only CCR1 was detected in the proteome of S-cultured AD-MSCs. CCR1 is a chemokine receptor with multiple ligands, i.e., CCL2, CCL3, CCL5, and CCL7. Currently, *in vitro* and *in vivo* evidence supports MSCs tissue homing via this receptor.[26] These results reinforce the observation that in our setting small-scale cultured AD-MSCs express a wide array of receptors possibly enabling tissue homing and immunomodulation potency.

MSCs immunosuppressive capacity is not constitutive; instead, it is induced by inflammatory cytokines, such as those in the inflammatory microenvironment.[27] In this study, AD-MSCs were not stimulated with any inflammatory insult. Therefore, future studies should address the effect that MSCs priming has on MSCs' properties after both S and L-scale expansion.

Another key property involved in tissue repair and regeneration is angiogenesis and ECM remodeling.[28,29] The angiogenic potential of MSCs is known to be produced by multiple soluble factors such as VEGF, FGF2, TGFB, IL-6, MCP1, and ANG-1.[30,31] We did not observe

Figure 3. Membrane-bound and intracellular proteome of adipose-derived mesenchymal stromal cells

(A) Principal-component analysis (PCA) of adipose-derived mesenchymal stromal cells cultured under either small scale (S) or large scale (L) conditions analyzed by mass spectrometry. The plot displays the clustering of each experiment, with *x* and *y* axes displaying the first two principal components, capturing 52.2% and 14.8% of the total variance of the dataset, respectively. (B) Heatmap displaying the relative abundances of differentially regulated proteins between small- and large scale culture conditions. Significance was determined by Student's two-sided t test, using *p*-values below 0.01 as a cutoff. Multiple testing correction was performed by permutation-based FDR correction, with an S0 value of 0.5. Hierarchical K-means clustering on rows (protein groups) and columns (donor samples) were performed by Euclidian distance, and the relative abundance of proteins are displayed as *Z* score normalized values for each protein group. (C) Heatmap of selected proteins and their associated functional pathways across each donor and culture condition. Relative protein abundances are displayed by *Z* score normalized valued across rows. (D) Pairwise Spearman correlation analysis between significantly regulated RNA transcripts and proteins. Significance of association was determined by testing the Spearman's coefficient for correlation between the mean fold-change values for each gene, *p*-value <2.2E−16.

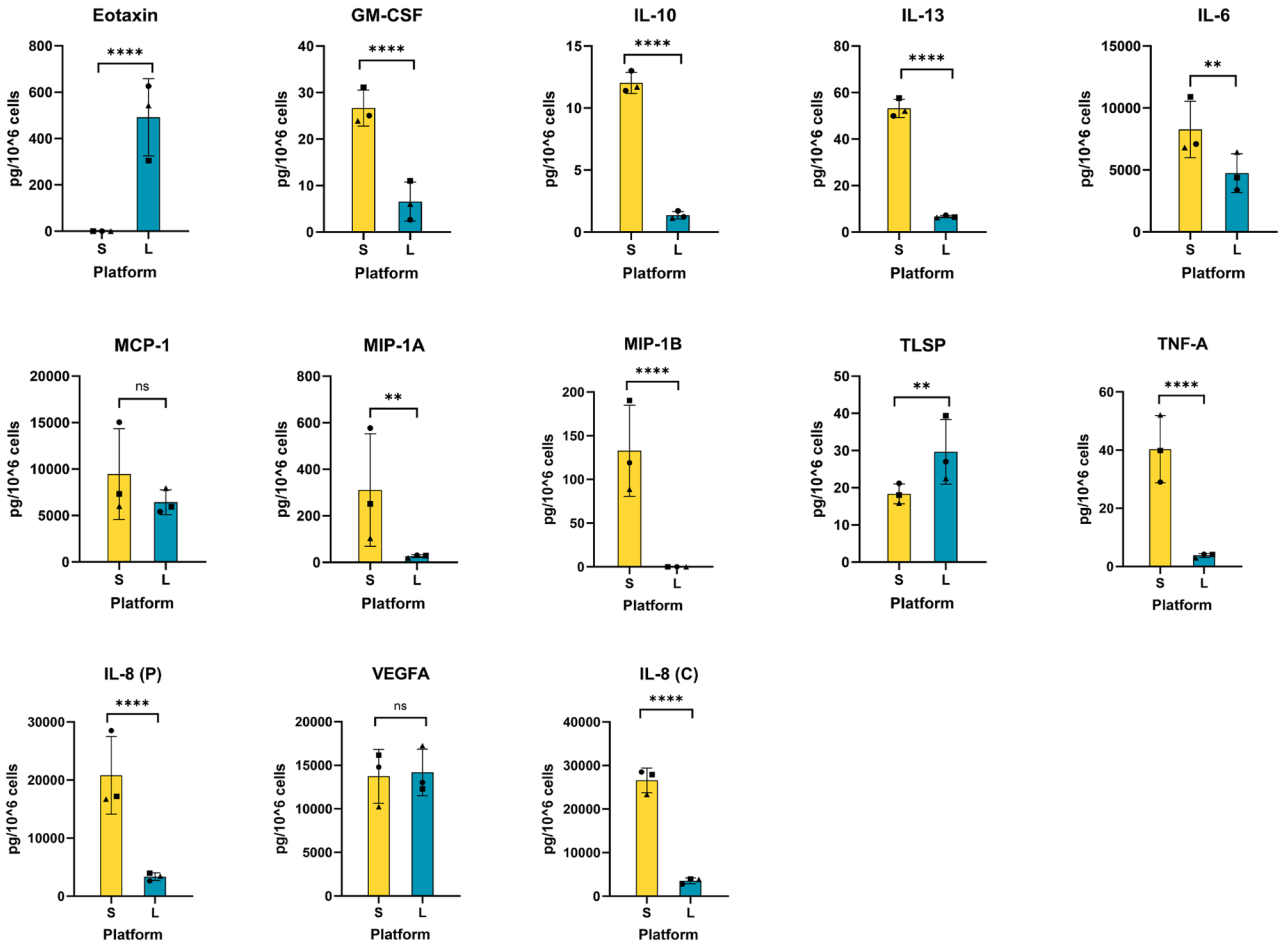

Figure 4. Influence of culture platform on a panel of secreted factors by AD- MSCs

Multiplex assay using Meso Scale Discovery (MSD) technology of secreted factors in the media expressed by AD-MSCs cultured in both platforms. (ns, not significant; *$p < 0.05$, **$p < 0.005$, and ****$p < 0.0001$).

a difference in VEGF-A, one of the main effector molecules in angiogenesis; however, we did observe some differences in their regulatory profiles. The observed discrepancy between VEGF-A transcriptional activity and secreted protein levels may suggest differences in post-transcriptional regulation or protein stability across platforms, warranting further investigation. When assessing pathways involved in ECM remodeling, transcriptional and proteomic levels showed that small scale cultured cells displayed a profile toward ECM degradation and remodeling with high expression of metalloproteases, while large-scale cultured AD-MSCs showed a more balanced profile that could favor not only ECM degradation but also synthesis and structural integrity with expression of several types of collagens and genes involved in ECM remodeling and synthesis.

The observed differences in transcriptional and proteomic landscapes between culture platforms likely stem from variations in the culture microenvironment. Although media formulation and oxygen tension setpoints remained constant, the transition from static to dynamic culture systems inherently affects nutrient availability and local oxygen tensions. Furthermore, the shift from flask surfaces to microcarrier-based expansion introduces variations in biomechanical stimuli and alters the cells' capacity to form complex cell-to-cell and surface interactions, which may also influence the paracrine signaling microenvironment. Previous studies have demonstrated that such alterations can modulate the expression of, for example, ECM components, particularly collagens, which aligns with our observations.[32–34]

These combined effects on gene expression, protein production, and secretory profiles could significantly impact the cells' therapeutic properties. In fact, recent advancements in AD-MSCs culture technologies have underscored how optimization of *in vitro* conditions can significantly influence not only the yield but also the therapeutic relevance of AD-MSCs in their potential for treating complex disorders such as diabetes and its complications.[35] Understanding these mechanisms is crucial for optimizing large-scale production processes while maintaining desired cellular characteristics.

It is important to acknowledge that donor-to-donor variability can influence the reproducibility of MSCs research. In this study, we used four donors for transcriptomics and proteomics analysis, which constitutes a relatively small cohort. While this variability was considered, the limited sample size makes it difficult to fully assess how it might influence the reproducibility of the findings across larger patient cohorts. Future studies should aim to address this by incorporating a broader range of donors to better evaluate its impact on reproducibility and the generalizability of the findings.

To evaluate whether platform-dependent differences will affect AD-MSCs' properties, validation through relevant potency assays would be necessary. Although the precise mechanisms of action for AD-MSCs in specific clinical applications is often not completely known, choosing relevant potency assays will be crucial for establishing correlations between platform-induced changes in cell properties and their potential impact on therapeutic efficacy. In addition, to fully understand how these molecular and functional differences translate into clinical outcomes, *in vivo* validation will be critical. Specifically, investigating how large-scale cultured MSCs perform in preclinical models of tissue repair and immune modulation will be crucial to better understand their behavior and therapeutic potential in clinical settings.

Our study emphasizes that translation from small-scale into large-scale cultures, or in general when switching culture platforms, warrants careful optimization and validation of production and culture processes to ensure the preservation of critical AD-MSCs attributes and potentially its therapeutic efficacy. The observed variation in cellular characteristics based on culture platform is essential to acknowledge in the context of clinical studies, where variations in cell production methods may contribute to differences in therapeutic outcomes. Future research should focus on developing appropriate methods to detect and mitigate the variability induced by different culture conditions, as well as developing standardized potency assays correlating platform-induced changes with therapeutic efficacy. In conclusion, our study underscores a potential new factor contributing to the limitations preventing clinical studies from advancing to late phases. Understanding this relationship is crucial for ensuring the quality and potency of high yield MSCs products, ultimately leading to clinically relevant outcomes.

MATERIALS AND METHODS

Cell isolation and culture expansion

Adipose tissue was collected from otherwise discarded material from elective cosmetic procedures. The lipoaspirate was processed in a GID SVF-2 system (GID Europe) to isolate the adipose-derived stem cells (ASCs) according to manufacturer's instructions. In brief, the isolation protocol involved enzymatic digestion using the manufacturer's collagenase formulation, with tissue incubation at 37°C for 75 min under continuous rotation. The stromal vascular fraction (SVF) was then pelleted by centrifugation at 600 g for 10 min. The resulting cell pellet was suspended in a growth medium comprising Dulbecco's modified Eagle's medium supplemented with 2 IU/mL heparin (preservative-free), 1% penicillin/streptomycin, and 8% pooled human platelet lysate (pHPL, sourced from PL Bioscience, Aachen, Germany).

For traditional adherent culture, SVF cells were cultured at approximately 5,000 cells per square centimeter in cell factories (NUNC, Thermo Fisher Scientific). The cultures were maintained in controlled atmospheric conditions (85% nitrogen, 10% oxygen, and 5% carbon dioxide) at 37°C using a BioSpherix Xvivo System X2 isolator (BioSpherix, Parish, NY). Following a two-week cultivation period, cells were harvested using TrypLE (Gibco, Thermo Fisher Scientific) enzymatic dissociation.

For bioreactor culture, 85×10^6 SVF cells were seeded in a bioreactor system (Eppendorf BioBlu/BioFlo320) and the cultures were maintained at controlled conditions (10% O_2 and 5% CO_2 [pH 7.4], 37°C). After 14 days in culture, the cells were harvested using a standard trypsinization protocol (TrypLE; Gibco, Thermo Fisher Scientific). Cells harvested from flask- and bioreactor-culture were counted using an NC-200 nuclecounter (Chemometec) and Via-1 cassettes containing acridine orange and 4′,6-diamidino-2-phenylindole (DAPI) stain. Live cell count was used to calculate fold increase, population doublings (PD = 3.322[log(cell yield)] − log[cell seed]) and PD time (PDt = PD/hours in culture).

Flow cytometry

AD-MSCs were washed and resuspended in fluorescence-activated cell sorting (FACS) buffer (PBS, 0.1 mM EDTA and 1% human albumin). Cells were incubated with an FC-blocking antibody mix (BioLegend) for 5 min before adding viability stain (7AAD, BioLegend) and, subsequently, single antibody mixture containing CD44-FITC, CD73-PE, CD90 FITC, and CD105-PE (Beckman Coulter), CD34-PE and CD31-FITC (BD Biosciences), CD45-FITC, or HLA-DR-APC (BioLegend), and incubating for 30 min at room temperature. The cells were washed once and subsequently resuspended in FACS buffer and analyzed on a Navios flow cytometer (Beckman Coulter). The flow cytometry data were analyzed using FlowJo software. The cell population was identified by FSC/SSC gating (forward scatter/side scatter), doublets discrimination, and live cells. Negative gates were established using unstained samples or fluorescence minus one (FMO) control. Positive gates were set to contain no negative signal.

Differentiation potential

ASCs were differentiated into adipocytes, chondrocytes, and osteoblasts in separate 12-well plates (NUNC, Thermo Fisher Scientific), according to manufacturer's instructions (StemPro Differentiation kit, Gibco). A density of 1×10^4 viable cells/cm^2 was seeded for adipogenesis and osteogenesis and 5 μL drop of $1{,}6 \times 10^6$ cell/mL for chondrogenesis. Pre-warmed differentiation media was refed every three days for 14 days (adipogenesis and chondrogenesis) and 21 days (osteogenesis). On the last day of cell culture, the cells were fixed with 4% formaldehyde solution for 10 min and specific colorimetric staining was performed.

In the adipogenesis plate, 60% isopropanol was added and removed after 5 min. Then, oil red working solution (1:3 dilution of oil red stock solution [0.5% oil red solution diluted to 0.3% in 99% isopropanol] and distilled water) was added and incubated for 5 more minutes, and then removed with rinsing water. In the osteogenesis plate, filtered alizarin red solution (2 g alizarin red in 90 mL distilled water with a final pH of 4.1–4.3) was added to the wells, incubated for 15 min, and washed 4 times with distilled water. In the chondrogenesis plate, filtered Alcian blue solution (pH 2.5) was added to the wells and incubated for 30 min. Wells were washed 3 times with 0.1M HCl and rinsed with Milli-Q water.

Bulk RNA-seq analysis

RNA was purified using QIAGEN RNeasy Mini Kit (QIAGEN), according to manufacturer's protocol. RNA purity was validated using a NanoDrop Spectrophotometer with A260/A280 and A260/A230 minimum criteria of 1.7–2.2. Samples were frozen at −80°C until sent for sequencing to BGI Europe Genome Center. BGI performed quality control (QC) test, polyA-selected and stranded mRNA library preparation, and PE100 sequencing with at least 20M pair reads per sample on DNA nanoball sequencing (DNBSEQ).

Further quality control on the raw RNA-seq data obtained for each individual sample was performed using FastQC (version 0.11.9).[36] An overview of the sequencing quality across all samples was visualized using MultiQC (version 1.13).[37] Subsequently, the raw reads were aligned to the human genome (GRCh38.p13, GENCODE Release 41 genome annotation)[38] using STAR (version 2.7.10b)[39] and post-alignment quality control was performed using Picard (version 2.27.5)[40] to ensure high-quality alignments. Raw expression counts per gene were extracted from STAR and used as an input to DEseq2 (version 1.42.1)[41] which was used to normalize the counts, perform statistical testing and differential expression analysis between samples of the small (S) and large (L) culture scale in R studio (version 4.3.0). DEGs were filtered using an adjusted p-value threshold of <0.05 applying Benjamini-Hochberg correction and a log2 fold change cutoff of |2|. Active-subnetwork-oriented pathway enrichment analysis was performed using pathfindR (version 2.3.1)[42] in R studio, leveraging interaction information from STRING protein-protein interaction network (version 12.0).[43] Consequently, we evaluated significantly enriched terms (pathways/gene sets) only for DEGs involved in active subnetworks (Table S2), focusing on Gene Ontology (GO)[44] gene sets of "biological process (BP)" and "molecular function (MF)" with a Benjamini-Hochberg adjusted p-value <0.05, retrieved over ten out of ten iterations (Table S3). The following R packages ("ggplot2," "ggalluvial," "ComplexHeatmap," "pathfindR," and "factoextra") were used for further statistical analysis and visualization of the transcriptomic data.

Sample preparation for mass spectrometry analysis

Acetone-precipitated protein pellets were resuspended in 100 µL of lysis buffer (1% sodium deoxycholate and 100 mM Tris-HCl [pH 8.5]) and incubated for 10 min at 99°C followed by two rounds of sonication using a Bioruptor pico (15 cycles, 30 s on/off, ultra-low frequency). Extracts were cleared by centrifugation, reduced with 5 mM (final concentration) Tris(2-carboxyethyl)phosphine (Tcep) for 15 min at 55°C, alkylated with 20 mM (final concentration) chloroacetamide (CAA) for 30 min at room temperature, and digested for 16 h at 37°C after adding trypsin and lysyl endopeptidase C (LysC) at 1:100 (enzyme:protein ratio). Peptides were acidified with 1% (final concentration) trifluoroacetic acid (TFA) and desalted using SDB-RPS StageTips.

Liquid chromatography-mass spectrometry analysis

Peptides were separated on an Aurora (Gen3) 25 cm, 75 µM ID column packed with C18 beads (1.7 µm) (IonOpticks) using a Vanquish Neo (Thermo Fisher Scientific) ultra-high-performance liquid chromatography (UHPLC). Peptide separation was performed using a 90-min gradient of 2%–17% solvent B (0.1% formic acid in acetonitrile) for 56 min, 17%–25% solvent B for 21 min, 25%–35% solvent B for 13 min, using a constant flow rate of 400 nL/min. Column temperature was maintained at 50°C. Upon elution, peptides were injected via a CaptiveSpray source and 20-µm emitter into a timsTOF HT mass spectrometer (Bruker) operated in diaPASEF mode. MS data were collected over a 100–1,700 m/z range. During each MS/MS data collection, each PASEF cycle was 1.8 s. Ion mobility was calibrated using three Agilent ESI-L Tuning Mix ions 622.0289, 922.0097, and 1221.9906. For diaPASEF, we used the long-gradient method which included 16 data-independent acquisition parallel accumulation–serial fragmentation (diaPASEF) scans with two 25 Da windows per ramp, mass range 400.0–1,201.0 Da, and mobility range 1.43–0.6 1/K0. The collision energy was decreased linearly from 59 eV at 1/K0 = 1.6 to 20 eV at 1/K0 = 0.6 Vs. cm2. Both accumulation time and PASEF ramp time were set to 100 ms.

MS data processing

Raw files were processed using DIA-NN 1.8.2 for data independent acquisition MS analysis.[45] The pipeline was executed using a cutoff of 0.01 false discovery rate (FDR) for proteins and precursors. The data was searched library free, using a human FASTA file to generate a spectral library. The minimum and maximum mass-to-charge ratio for fragments was 200–1,800 m/z, respectively. We considered all tryptic peptides with up to one missing cleavage, and allowed for N-terminal methionine excision. Resulting peptides were included in the search space with lengths from 7 to 30 amino acids, with precursor mass-to-charge ratios ranging from 300 to 1,800 m/z, with charge states 1–4. We searched with cysteine carbamidomethylation enabled as a fixed modification, and allowed for 4 variable modifications per peptide, considering methionine oxidation and acetylation of the N-terminus. We enabled smart profiling and heuristic protein inference.

Bioinformatics and statistical analysis

The raw DIA-NN protein group matrix outputs were analyzed using the statistical programming language R (version 4.3.1 "Beagle Scouts") and the Perseus software suite.[46,47] Briefly, the intensities

were log2 transformed, quality filtered to ensure no missing values within at least one group, followed by imputation of missing values under the assumption missing not at random by randomly sampling of a downshifted normal distribution separately for each column (width 0.3, mean downshift 1.8). The significance of DEPs was determined using Student's t test, with a threshold of 1% for *p*-values, which were controlled for multiple-hypothesis testing by permutation-based FDR correction. GSEA was performed using multiple Fisher's exact tests with Benjamini-Hochberg multiple-hypothesis correction applied to test for enriched terms, setting a *p*-value threshold at 1%. PCA was performed in R using the prcomp function.

Data integration between transcriptomics and DIA proteomics data was performed by mapping differentially regulated genes determined by RNA-seq analysis onto the proteomics data frame, matching by gene names. In case different genes would match the same within the same protein group, the mean log2 fold changes were transferred for those genes. Pearson correlation between differentially regulated genes found by transcriptomics and proteomics was determined using the cor.test() function. Heatmap with selected proteins and their functional annotations were made by plotting their *Z* score normalized proteomics intensities following their transformation and filtering, as previously described.

Meso scale multiplex ELISA

When cells were harvested on day 14, supernatant samples were collected from flask- and bioreactor-based cultures and cryopreserved at −80°C. Cryopreserved aliquots of supernatants from cell cultures were thawed in a 37°C water bath. Culture media containing 10% pHPL was included as a reference. Commercially available V-PLEX human biomarker panels (chemokine-1, cytokine-1, cytokine-2, proinflammatory-1, and vascular injury-2; Meso Scale Discovery, USA) were used to quantify released factors: eotaxin, eotaxin-3, IL-8, IP-10, MCP-1, MCP-4, MDC, MIP-1A, MIP-1B, TARC, GM-CSF, IL-12, IL-15, IL-16, IL-17A, IL-1A, IL-5, IL-7, TNF-β, VEGF, IL-17A/F, IL-17B, IL-17C, IL-17D, IL-1RA, IL-3, IL-9, TLSP, IFN-γ, IL-10, IL-12p70, IL-13, IL-1β, IL-2, IL-4, IL-6, IL-8, TNF-α, CRP, SAA, ICAM-1, and vCAM-1. The assays were performed according to manufacturer's instructions, using the dilutions recommended for plasma. The MESO QuickPlex SQ 120 instrument was used to collect data, which were then analyzed using the accompanying DISCOVERY WORKBENCH software.

Statistical analyses

Statistical analyses for cell yield, PD and PD time (PDT) as well as for MSD cytokine panel, were conducted using GraphPad Prism version 7. Data were obtained from experiments performed using four independent donors, each contributing to both small and large culture platforms groups. Paired t tests were used to compare yield, PD, and PD time (PDT) between the two groups. For the analysis of MSD (mean square displacement) graphs, a two-way analysis of variance (two-way ANOVA) was applied to evaluate the effects of the culture method and other experimental conditions. Error bars in all graphs represent the standard deviation (SD). Statistical significance was determined using a threshold *p*-value of <0.05.

DATA AVAILABILITY

All the data generated in this study are included in this article and in its supplementary files. The mass spectrometry proteomics data have been deposited to the ProteomeXchange Consortium via the PRIDE partner repository with the dataset identifier PXD058625.[48]

ACKNOWLEDGMENTS

We would like to extend our gratitude to a PhD student grant for M.R.G. from the LEO Foundation through the LEO Foundation Skin Immunology Research Center (award no. LF18500). We also like to thank Julie Nygaard and Signe Ilsoe for their excellent technical assistance with cell culture and sample collection. Mass spectrometry based proteomics analyses were performed by the Proteomics Research Infrastructure (PRI) at the University of Copenhagen (UCPH), supported by the Novo Nordisk Foundation (NNF) (grant agreement no. NNF19SA0059305).

All patients gave written informed consent to the treatment. The project was performed on discarded biological material obtained from anonymous donors and was therefore not registered by the local Ethical Committee, which is in accordance with the Danish Legislation on Ethic in Health Science.

AUTHOR CONTRIBUTIONS

M.R.G., A.W., and J.S. designed the research. M.R.G. and J.S. performed the experiments. M.R.G., J.S., A.W., A.O., and J.D.E. analyzed and interpreted the data, made the figures, and wrote the original draft of the paper. A.O. analyzed and made figures for the transcriptomic data. B.D. and M.B.L. prepared samples and run LC-MS analysis for the mass spectrometry samples. J.D.E. analyzed and made figures for the proteomic data. A.F.-N., L.M.F., L.H., F.I., B.D., and M.B.L. reviewed and edited the manuscript. L.M.F., F.I., and A.W. contributed to the interpretation of data and provided critical revisions during manuscript preparation. A.W. and J.S. acquired the funding and supervised the project. All authors have read and agreed to the published version of the manuscript.

DECLARATION OF INTERESTS

This study was partially funded by Celcore. J.D.S., L.M.F., and A.F.-N. are employees of Celcore and were involved in study design, execution, data analysis, and manuscript preparation. The authors declare that this commercial affiliation does not alter their adherence to scientific standards and principles.

SUPPLEMENTAL INFORMATION

Supplemental information can be found online at https://doi.org/10.1016/j.omtm.2025.101512.

REFERENCES

1. Shi, Y., Su, J., Roberts, A.I., Shou, P., Rabson, A.B., and Ren, G. (2012). How mesenchymal stem cells interact with tissue immune responses. Trends Immunol. *33*, 136–143.

2. Huang, Y., Wu, Q., and Tam, P.K.H. (2022). Immunomodulatory Mechanisms of Mesenchymal Stem Cells and Their Potential Clinical Applications. Int. J. Mol. Sci. *23*, 10023.

3. Zhou, T., Yuan, Z., Weng, J., Pei, D., Du, X., He, C., and Lai, P. (2021). Challenges and advances in clinical applications of mesenchymal stromal cells. J. Hematol. Oncol. *14*, 24.

4. Wu, X., Jiang, J., Gu, Z., Zhang, J., Chen, Y., and Liu, X. (2020). Mesenchymal stromal cell therapies: Immunomodulatory properties and clinical progress. Stem Cell Res. Ther. *11*, 345.

5. Bernardo, M.E., and Fibbe, W.E. (2013). Mesenchymal stromal cells: Sensors and switchers of inflammation. Cell Stem Cell *13*, 392–402. https://doi.org/10.1016/j.stem.2013.09.006.

6. Galipeau, J., and Sensébé, L. (2018). Mesenchymal Stromal Cells: Clinical Challenges and Therapeutic Opportunities. Cell Stem Cell *22*, 824–833.

7. Krampera, M., and Le Blanc, K. (2021). Mesenchymal stromal cells: Putative microenvironmental modulators become cell therapy. Cell Stem Cell *28*, 1708–1725.

8. Ma, T., Tsai, A.C., and Liu, Y. (2016). Biomanufacturing of human mesenchymal stem cells in cell therapy: Influence of microenvironment on scalable expansion in bioreactors. Biochem. Eng. J. *108*, 44–50.

9. Mizukami, A., Fernandes-Platzgummer, A., Carmelo, J.G., Swiech, K., Covas, D.T., Cabral, J.M.S., and da Silva, C.L. (2016). Stirred tank bioreactor culture combined with serum-/xenogeneic-free culture medium enables an efficient expansion of umbilical cord-derived mesenchymal stem/stromal cells. Biotechnol. J. *11*, 1048–1059.

10. Simão, V.A., Brand, H., da Silveira-Antunes, R.N., Fukasawa, J.T., Leme, J., Tonso, A., and Ribeiro-Paes, J.T. (2023). Adipose-derived stem cells (ASCs) culture in spinner flask: improving the parameters of culture in a microcarrier-based system. Biotechnol. Lett. *45*, 823–846.

11. Rafiq, Q.A., Brosnan, K.M., Coopman, K., Nienow, A.W., and Hewitt, C.J. (2013). Culture of human mesenchymal stem cells on microcarriers in a 5 l stirred-tank bioreactor. Biotechnol. Lett. *35*, 1233–1245.

12. Teixeira, F.G., Panchalingam, K.M., Assunção-Silva, R., Serra, S.C., Mendes-Pinheiro, B., Patrício, P., Jung, S., Anjo, S.I., Manadas, B., Pinto, L., et al. (2016). Modulation of the Mesenchymal Stem Cell Secretome Using Computer-Controlled Bioreactors: Impact on Neuronal Cell Proliferation, Survival and Differentiation. Sci. Rep. *6*, 27791.

13. Caruso, S.R., Orellana, M.D., Mizukami, A., Fernandes, T.R., Fontes, A.M., Suazo, C.A.T., Oliveira, V.C., Covas, D.T., and Swiech, K. (2014). Growth and functional harvesting of human mesenchymal stromal cells cultured on a microcarrier-based system. Biotechnol. Prog. *30*, 889–895.

14. Bourin, P., Bunnell, B.A., Casteilla, L., Dominici, M., Katz, A.J., March, K.L., Redl, H., Rubin, J.P., Yoshimura, K., and Gimble, J.M. (2013). Stromal cells from the adipose tissue-derived stromal vascular fraction and culture expanded adipose tissue-derived stromal/stem cells: A joint statement of the International Federation for Adipose Therapeutics and Science (IFATS) and the International Society for Cellular Therapy (ISCT). Cytotherapy *15*, 641–648.

15. Dominici, M., Le Blanc, K., Mueller, I., Slaper-Cortenbach, I., Marini, F., Krause, D., Deans, R., Keating, A., Prockop, D., and Horwitz, E. (2006). Minimal criteria for defining multipotent mesenchymal stromal cells. The International Society for Cellular Therapy position statement. Cytotherapy *8*, 315–317.

16. Potente, M., Gerhardt, H., and Carmeliet, P. (2011). Basic and therapeutic aspects of angiogenesis. Cell *146*, 873–887. https://doi.org/10.1016/j.cell.2011.08.039.

17. Bronckaers, A., Hilkens, P., Martens, W., Gervois, P., Ratajczak, J., Struys, T., and Lambrichts, I. (2014). Mesenchymal stem/stromal cells as a pharmacological and therapeutic approach to accelerate angiogenesis. Pharmacol. Ther. *143*, 181–196. https://doi.org/10.1016/j.pharmthera.2014.02.013.

18. Chinnadurai, R., Rajan, D., Qayed, M., Arafat, D., Garcia, M., Liu, Y., Kugathasan, S., Anderson, L.J., Gibson, G., and Galipeau, J. (2018). Potency Analysis of Mesenchymal Stromal Cells Using a Combinatorial Assay Matrix Approach. Cell Rep. *22*, 2504–2517.

19. Song, N., Scholtemeijer, M., and Shah, K. (2020). Mesenchymal Stem Cell Immunomodulation: Mechanisms and Therapeutic Potential. Trends Pharmacol. Sci. *41*, 653–664. https://doi.org/10.1016/j.tips.2020.06.009.

20. Tompkins, B.A., DiFede, D.L., Khan, A., Landin, A.M., Schulman, I.H., Pujol, M.V., Heldman, A.W., Miki, R., Goldschmidt-Clermont, P.J., Goldstein, B.J., et al. (2017). Allogeneic Mesenchymal Stem Cells Ameliorate Aging Frailty: A Phase II Randomized, Double-Blind, Placebo-Controlled Clinical Trial. J. Gerontol. A Biol. Sci. Med. Sci. *72*, 1513–1522.

21. Gavin, C., Meinke, S., Heldring, N., Heck, K.A., Achour, A., Iacobaeus, E., Höglund, P., Le Blanc, K., and Kadri, N. (2019). The Complement System Is Essential for the Phagocytosis of Mesenchymal Stromal Cells by Monocytes. Front. Immunol. *10*, 2249.

22. Machado, C.d.V., Telles, P.D.d.S., and Nascimento, I.L.O. (2013). Immunological characteristics of mesenchymal stem cells. Rev. Bras. Hematol. Hemoter. *35*, 62–67. https://doi.org/10.5581/1516-8484.20130017.

23. van Megen, K.M., van 't Wout, E.J.T., Lages Motta, J., Dekker, B., Nikolic, T., and Roep, B.O. (2019). Activated Mesenchymal Stromal Cells Process and Present Antigens Regulating Adaptive Immunity. Front. Immunol. *10*, 694.

24. Wang, Y., Chen, X., Cao, W., and Shi, Y. (2014). Plasticity of mesenchymal stem cells in immunomodulation: Pathological and therapeutic implications. Nat. Immunol. *15*, 1009–1016. https://doi.org/10.1038/ni.3002.

25. Andreas, K., Sittinger, M., and Ringe, J. (2014). Toward in situ tissue engineering: Chemokine-guided stem cell recruitment. Trends Biotechnol. *32*, 483–492. https://doi.org/10.1016/j.tibtech.2014.06.008.

26. Shan, Y., Zhang, M., Tao, E., Wang, J., Wei, N., Lu, Y., Liu, Q., Hao, K., Zhou, F., and Wang, G. (2024). Pharmacokinetic characteristics of mesenchymal stem cells in translational challenges. Signal Transduct. Target. Ther. *9*, 242. https://doi.org/10.1038/s41392-024-01936-8.

27. Ren, G., Zhang, L., Zhao, X., Xu, G., Zhang, Y., Roberts, A.I., Zhao, R.C., and Shi, Y. (2008). Mesenchymal Stem Cell-Mediated Immunosuppression Occurs via Concerted Action of Chemokines and Nitric Oxide. Cell Stem Cell *2*, 141–150.

28. Guillamat-Prats, R. (2021). The role of MSC in wound healing, scarring and regeneration. Cells *10*, 1729. https://doi.org/10.3390/cells10071729.

29. Riedl, J., Popp, C., Eide, C., Ebens, C., and Tolar, J. (2021). Mesenchymal stromal cells in wound healing applications: role of the secretome, targeted delivery and impact on recessive dystrophic epidermolysis bullosa treatment. Cytotherapy *23*, 961–973. https://doi.org/10.1016/j.jcyt.2021.06.004.

30. Kwon, H.M., Hur, S.M., Park, K.Y., Kim, C.K., Kim, Y.M., Kim, H.S., Shin, H.C., Won, M.H., Ha, K.S., Kwon, Y.G., et al. (2014). Multiple paracrine factors secreted by mesenchymal stem cells contribute to angiogenesis. Vascul. Pharmacol. *63*, 19–28.

31. Tao, H., Han, Z., Han, Z.C., and Li, Z. (2016). Proangiogenic Features of Mesenchymal Stem Cells and Their Therapeutic Applications. Stem Cells Int. *2016*, 1314709. https://doi.org/10.1155/2016/1314709.

32. Sun, Y., Wan, B., Wang, R., Zhang, B., Luo, P., Wang, D., Nie, J.J., Chen, D., and Wu, X. (2022). Mechanical Stimulation on Mesenchymal Stem Cells and Surrounding Microenvironments in Bone Regeneration: Regulations and Applications. Front. Cell Dev. Biol. *10*, 808303. https://doi.org/10.3389/fcell.2022.808303.

33. Baker, B.M., and Chen, C.S. (2012). Deconstructing the third dimension-how 3D culture microenvironments alter cellular cues. J. Cell Sci. *125*, 3015–3024. https://doi.org/10.1242/jcs.079509.

34. Discher, D.E., Mooney, D.J., and Zandstra, P.W. (2009). Growth factors, matrices, and forces combine and control stem cells. Science *324*, 1673–1677.

35. Shi, Y., Yang, X., Min, J., Kong, W., Hu, X., Zhang, J., and Chen, L. (2024). Advancements in culture technology of adipose-derived stromal/stem cells: implications for diabetes and its complications. Front. Endocrinol. *15*, 1343255. https://doi.org/10.3389/fendo.2024.1343255.

36. Andrews, S. (2010). FastQC: a quality control tool for high throughput sequence data. http://www.bioinformatics.babraham.ac.uk/projects/fastqc.

37. Ewels, P., Magnusson, M., Lundin, S., and Käller, M. (2016). MultiQC: Summarize analysis results for multiple tools and samples in a single report. Bioinformatics *32*, 3047–3048.

38. Frankish, A., Carbonell-Sala, S., Diekhans, M., Jungreis, I., Loveland, J.E., Mudge, J.M., Sisu, C., Wright, J.C., Arnan, C., Barnes, I., et al. (2023). GENCODE: reference annotation for the human and mouse genomes in 2023. Nucleic Acids Res. *51*, D942–D949.

39. Dobin, A., Davis, C.A., Schlesinger, F., Drenkow, J., Zaleski, C., Jha, S., Batut, P., Chaisson, M., and Gingeras, T.R. (2013). STAR: Ultrafast universal RNA-seq aligner. Bioinformatics *29*, 15–21.

40. Broad Institute (2024). Picard Tools Documentation. https://broadinstitute.github.io/picard/.

41. Love, M.I., Huber, W., and Anders, S. (2014). Moderated estimation of fold change and dispersion for RNA-seq data with DESeq2. Genome Biol. *15*, 550.

42. Ulgen, E., Ozisik, O., and Sezerman, O.U. (2019). PathfindR: An R package for comprehensive identification of enriched pathways in omics data through active subnetworks. Front. Genet. *10*, 858.

43. Szklarczyk, D., Kirsch, R., Koutrouli, M., Nastou, K., Mehryary, F., Hachilif, R., Gable, A.L., Fang, T., Doncheva, N.T., Pyysalo, S., et al. (2023). The STRING database in 2023: protein-protein association networks and functional enrichment analyses for any sequenced genome of interest. Nucleic Acids Res. *51*, D638–D646.

44. The Gene Ontology Consortium (2019). The Gene Ontology Resource: 20 years and still GOing strong. Nucleic Acids Res. *47*, D330–D338.

45. Demichev, V., Messner, C.B., Vernardis, S.I., Lilley, K.S., and Ralser, M. (2020). DIA-NN: neural networks and interference correction enable deep proteome coverage in high throughput. Nat. Methods *17*, 41–44.

46. Goss Tusher, V., Tibshirani, R., and Chu, G. (2021). Significance Analysis of Microarrays Applied to the Ionizing Radiation Response. Proc. Natl. Acad. Sci. USA *98*, 5116–5121. https://doi.org/10.1073/pnas.091062498.

47. Tyanova, S., Temu, T., Sinitcyn, P., Carlson, A., Hein, M.Y., Geiger, T., Mann, M., and Cox, J. (2016). The Perseus computational platform for comprehensive analysis of (prote)omics data. Nat. Methods *13*, 731–740. https://doi.org/10.1038/nmeth.3901.

48. Perez-Riverol, Y., Bai, J., Bandla, C., García-Seisdedos, D., Hewapathirana, S., Kamatchinathan, S., Kundu, D.J., Prakash, A., Frericks-Zipper, A., Eisenacher, M., et al. (2022). The PRIDE database resources in 2022: A hub for mass spectrometry-based proteomics evidences. Nucleic Acids Res. *50*, D543–D552.